

Article

Electrochemical Characteristics of Amorphous Ni-P Electroplated Thin Film

Jae-Young Hong  and Heon-Cheol Shin *

School of Materials Science and Engineering, Pusan National University, Busan 46241, Korea; hjy9702@naver.com

* Correspondence: hcshin@pusan.ac.kr; Tel.: +82-51-510-3099; Fax: +82-51-512-0528

Abstract: In this study, an amorphous nickel-phosphide (Ni-P) thin film was produced by electroplating, and its possible use as the anode material of a secondary lithium battery was explored. First, by changing the electroplating conditions, we created uniform and flat Ni-P thin films that contained 16–28 at% phosphorus. An evaluation of the manufactured thin film as anode material showed that a thin film with more phosphorus content had a higher specific discharge capacity. In particular, the initial gravimetric capacity of the electrode with the highest phosphorus content (28 at%) was comparable to that of graphite, but it had three times the initial volumetric capacity. The cycling stability improved with a higher phosphorus content. It was suggested that the adhesive strength between the substrate and thin film had a greater impact on the cycling stability than the physical damage caused by the volume changes during charging and discharging. To improve the specific capacity, we formed globular electrodeposits on the surface of the thin film. As a result, a discharge capacity comparable to the theoretical capacity of Ni-P was obtained, and the rate performance was additionally improved, without reduction in the life cycle.

Keywords: electrodeposition; nickel phosphide; phosphorus content; lithium battery; anode



Citation: Hong, J.-Y.; Shin, H.-C. Electrochemical Characteristics of Amorphous Ni-P Electroplated Thin Film. *Appl. Sci.* **2022**, *12*, 5951. <https://doi.org/10.3390/app12125951>

Academic Editors: Fernando B. Naranjo and Susana Fernández

Received: 13 May 2022

Accepted: 10 June 2022

Published: 11 June 2022

Publisher's Note: MDPI stays neutral with regard to jurisdictional claims in published maps and institutional affiliations.



Copyright: © 2022 by the authors. Licensee MDPI, Basel, Switzerland. This article is an open access article distributed under the terms and conditions of the Creative Commons Attribution (CC BY) license (<https://creativecommons.org/licenses/by/4.0/>).

1. Introduction

Currently, secondary batteries are receiving significant attention as core energy storage systems to realize a hyper-connected society in the 4th industrial revolution. Especially, lithium secondary batteries are gaining a special attention as power sources due to their high energy and power densities. In terms of the production cost and performance of lithium secondary batteries, studies on the four major components, such as the positive electrode, negative electrode, separator, and electrolyte, are mainly being conducted. In particular, research studies on positive and negative active materials, which have the most significant influence on the capacity and cycle life, are being most actively carried out [1–5].

From the anode perspective, the goal is to obtain a next-generation high-capacity active material that exceeds the specific capacity of graphite (372 mAh g^{-1}), which is currently in use [6]. For this purpose, various types of elements such as silicon, tin [7], sulfur [8,9], and phosphorus [10] are being studied as promising candidates. They all have high specific capacities, but there are critical disadvantages; they have low cycling stability because the active materials are mechanically broken down as a result of a significant volume change during charging and discharging. They also have inferior high-rate characteristics due to their relatively low electronic conductivities. Various methods are being used to figure out these issues, including mixing silicon with carbon materials or manipulating the microstructure/morphology of silicon to enhance the cycling stability [11]. Some studies have focused on compounds such as oxides, fluorides, sulfides, and phosphides to improve the conductivity and cycle life [8,12–16].

Among the next-generation negative active materials, transition metal phosphides (M-P, M = Ni [14], Fe [17], Co [18], Cu [19], etc.) are known to be combined with one phosphorus atom and three lithium atoms through a conversion mechanism ($\text{MP}_y + 3\text{yLi}^+$

+ 3ye⁻ ↔ yLi₃P + M⁰), and these have much higher theoretical specific capacities than that of the graphite. In addition, the M-P bond can be broken relatively easily and can react with lithium, and the degree of polarization is approximately 0.4 V in a typical charge–discharge situation. These have an advantage because the reaction polarization is lower than those of metal oxides (~0.9 V), metal fluorides (~1.1 V), and metal sulfides (~0.7 V) [20]. They also react with lithium at a narrow range of low voltages, making them more suitable for configuring high-voltage batteries [21,22].

Nickel phosphide (Ni-P) has high utilization among the transition metal phosphides because it can form various stable phases [23]. In particular, NiP₂ is known to react reversibly with lithium as a lithium battery anode [21,22,24,25]. Gillot et al. reported that their NiP₂ anode had an initial specific capacity of 1250 mAh g⁻¹, which was close to the theoretical capacity, and maintained a capacity of 800 mAh g⁻¹ after ten cycles [21]. Boyanov et al. also reported that a NiP₂ anode reacted reversibly with five lithium atoms [22]. However, Ni-P shows low coulombic efficiency due to significant capacity loss in the first cycle. In addition, there is still an issue with the deterioration of the cycling stability caused by a volume change, and its high-rate features are not as good as those of graphite [2,22,26,27]. To overcome this, particularly from the perspective of the nanostructure, studies related to the Ni-P anode active material are being widely conducted [10,14,15,21,25,27–31].

Most Ni-P crystalline materials are synthesized using the hot injection [28] and phosphorization methods [29]. However, these synthesis methods require a high-temperature environment of 300 °C or more, as well as complicated devices, and it is difficult to control the particle size distribution of Ni-P powder [32]. On the other hand, the device required for the electroplating method is relatively inexpensive [33–35], and it is possible to synthesize an anode in the form of a thin film [32,36,37]. In addition, because the composition and microstructure can be easily controlled by adjusting the plating conditions [38–40], it is viable to synthesize Ni-P with suitable characteristics for the application.

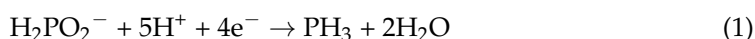
When synthesizing Ni-P using electroplating, as the phosphorus content increases, more phosphorus penetrates the nickel lattice, making the Ni-P deviate from the crystalline structure. When the phosphorus content is above a certain value (14–20 at%), it becomes an amorphous crystal structure [23,41]. As reported [17,42–46], amorphous structures exhibit a faster conversion–reaction rate than the corresponding crystalline structures. Gue et al. reported that the cycling stability of an amorphous MnO_x anode was improved because it had less deformation than a crystalline anode when it reacted with lithium, suggesting that amorphous materials could enhance the structural stability [42].

In this work, Ni-P amorphous thin films with different phosphorus contents were synthesized using electrolytic plating and tested as negative active materials for secondary lithium batteries. In particular, uniform Ni-P thin films containing 16–28 at% phosphorus were obtained at different plating conditions. To explore the possible use of amorphous Ni-P as an anode for a secondary battery, the initial characteristics (charge and discharge capacities, coulombic efficiency) and cycling stability were analyzed. In addition, the effect of surface morphology on the electrode performance was exploited by creating the globular electrodeposits on the surface of the thin film with a high phosphorus content.

2. Experimental Procedure

2.1. Preparation of Ni-P Thin Films Using Electroplating

Ni-P is known to be electroplated through the below indirect mechanism [47].



That is, Ni-P (Equations (1) and (2)) is concurrently coated with pure Ni (Equation (3)), and at the same time, H₂ evolution occurs (Equation (4)). In this study, Ni-P thin films were electrolytically plated using a three-electrode electrochemical cell. A copper foil (99.8%; Alfa

aesar, Haverhill, MA, USA) with a thickness of 20 μm was selected as a substrate and masked so that its exposed area was 1 cm^2 , and this was used as a working electrode. To remove the native oxide layer from the surface of the copper substrate, it was pretreated in 2.5 M H_2SO_4 (98%; Daejeong, Siheung-si, Gyeonggi-do, Korea) for 10 s and then washed with distilled water. A 6 cm^2 platinum metal plate was used as the counter electrode, and a saturated calomel electrode (SCE) was used as the reference electrode. To form the plating solution, 0.6 M $\text{NiSO}_4 \cdot 6\text{H}_2\text{O}$ (Cryst./Certified ACS; Fisher chemical), 0.2 M $\text{NiCl}_2 \cdot 6\text{H}_2\text{O}$ (Cryst./Certified; Fisher chemical), 0.1–1.8 M H_3PO_3 (98+%; Alfa aesar, Haverhill, MA, USA), and 0.6 M H_3PO_4 (85%; Junsei chemical, Tokyo, Japan) were used. Then, 3 M NaOH (97%; Junsei chemical, Tokyo, Japan) or ammonia water (35%; Alfa aesar, Haverhill, MA, USA) was added to adjust the acidity of the plating solution. All the electrolytic plating was performed at 60 °C. With stirring, the hydrogen gas generated during plating was removed from the electrode surface. The reduction current density was 40–100 mA cm^{-2} , and the thickness of all the plating layers was adjusted to be approximately 100 nm by controlling the plating time. In particular, the phosphorus content of the Ni-P thin film was determined by the H_3PO_3 concentration, reduction current density, and plating solution acidity [48]. Table 1 lists the plating conditions used in this study, along with the designations of the specimens.

Table 1. Preparation conditions of nickel phosphide thin films.

Sample Number	pH Adjuster	Denomination	Concentration of P Source (M)	pH	Current Density (mA cm^{-2})	Electrodeposition Time (s)
1	Ammonium hydroxide	P16	0.1	2.0	−100	5
2		P21	0.2	2.0	−80	10
3		P28	0.6	2.0	−40	30
4	3M NaOH	P28_S	1.8	1.5	−40	50

This work tried to indirectly confirm the adhesive strength by observing whether the film on the substrate maintained its structural integrity when the thin film was bent. The bending test was carried out by manually wrapping a structural body of copper with a 80 μm diameter cylindrical edge with the Ni-P thin film sample. After bending and straightening, the morphology of the part of the thin film that was bent was observed with an electron microscope. Bending speed was about one cycle per second.

The electroplating of the Ni-P thin films was conducted using an Iviumstat (Ivium technologies, The Netherlands). The morphology of the electroplated Ni-P thin films was analyzed using field-emission scanning electron microscopy (FE-SEM; MIRA3; TESCAN, Brno, Czech Republic), and the composition was verified using an energy-dispersive X-ray spectrometer (EDS; 51-XMZ1004; Oxford instruments, Abingdon, UK). The crystal structure of the thin film was identified using an X-ray diffractometer (XRD; Ultima-IV, Rigaku, Tokyo, Japan).

2.2. Evaluation of Electrochemical Properties as Negative Electrodes for Secondary Lithium Batteries

A two-electrode half cell was built to evaluate the electrochemical characteristics of the Ni-P electrodes synthesized under four different plating conditions. The half cell was fabricated in a glove box (Glove box; Mbraun-Unilab, Garching, Germany) in a high-purity Ar atmosphere. The oxygen and moisture concentrations were maintained below 0.1 ppm during cell fabrication and evaluation. A Ni-P electrode was used as a working electrode, and 16 Φ lithium foil was used as a counter electrode. A polypropylene separator (Celgard 2400) with a thickness of 25 μm was used by cutting it at 23 Φ , and 1 M LiPF_6 in ethylene carbonate: ethyl methyl carbonate at a 3:7 (vol%) ratio was used as the electrolyte. After fabricating the two-electrode half cell, a 3 h rest was provided for electrode soaking and interfacial stabilization. Then, the electrochemical properties were evaluated.

To verify the specific capacity, coulombic efficiency, and cycle characteristics of the Ni-P electrode as the negative electrode for a lithium-ion battery, it was charged and discharged at a 0.2 C rate at the potential range of 0.02–3 V vs. Li^+/Li (here, n C rate means that the charge/discharge current fully charges/discharges the electrode in

1/n h). To calculate the specific capacity of the electrode, the mass of the plated Ni-P thin film was obtained by subtracting the mass of the substrate before plating from the mass of the electrode after plating. When evaluating the high-rate characteristics, first, the effect of the irreversible capacity was excluded by charging and discharging twice at a 0.2 C rate; then, the rate performance tests were performed three times each while increasing the charge and discharge rates in the order of 0.2, 0.5, and 1 C rates. Finally, the test was performed three times at the initial 0.2 C rate. The capacity retention was calculated using the specific discharge capacity. The experiment was conducted using a VMP3 system (Biologic Co., Seyssinet-Pariset, France).

3. Results and Discussion

3.1. Morphology, Structure, and Composition of Ni-P Thin Films

Figure 1 shows the FE-SEM images of the Ni-P thin films (P16, P21, and P28) presented in Table 1. The P16, P21, and P28 thin films contained phosphorus at 16, 21, and 28 at%, respectively, as shown in the composition analysis results (Figure 2a–c). A flat and uniform Ni-P thin film was formed on the substrate in all three cases. From the inset figure of Figure 1, representing the inclined view of the thin film, it was confirmed that all the thin films had a thickness of approximately 100 nm. It is noted that no interfacial cracks between the thin film and substrate were observed in the P28 thin film, while interfacial cracking became more severe as the phosphorus content decreased (see the cracks indicated by the arrow in the inset of Figure 1a,b). The plating metal (Ni) and substrate metal (Cu) have high crystallographic similarities, and plating proceeded at a relatively high temperature (60 °C). Therefore, the consistency and adhesion between the thin film and substrate were expected to be superior [49]. However, a higher reduction current density applied when a thin film with a lower phosphorus content was created resulted in more hydrogen being generated at the substrate surface. As this hydrogen was adsorbed, more voids were likely to form between the substrate and thin film [50]. These interface voids and contact inferiority could decrease the adhesion between the substrate and thin film.

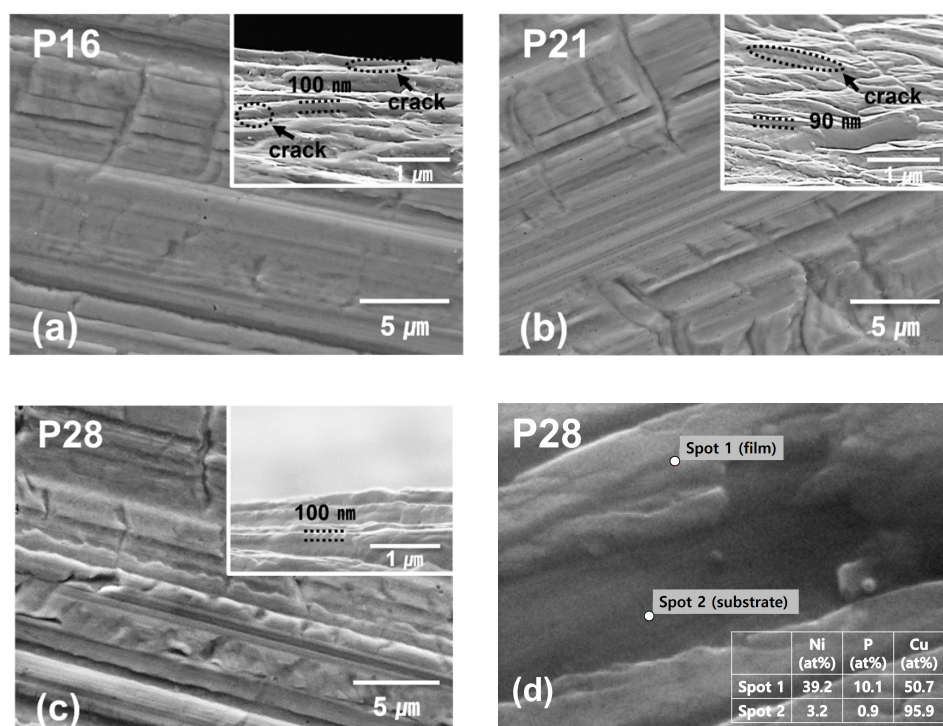


Figure 1. Scanning electron micrographs of the nickel phosphide thin films with different phosphorus (P) contents: (a) sample P16 (16 at% P), (b) sample P21 (21 at% P), and (c) sample P28 (28 at% P) in Table 1. Inset figures are the magnified inclined images. (d) represents the magnified image and composition of Ni-P electrodeposits (spot 1) and Cu substrate (spot 2) in sample P28.

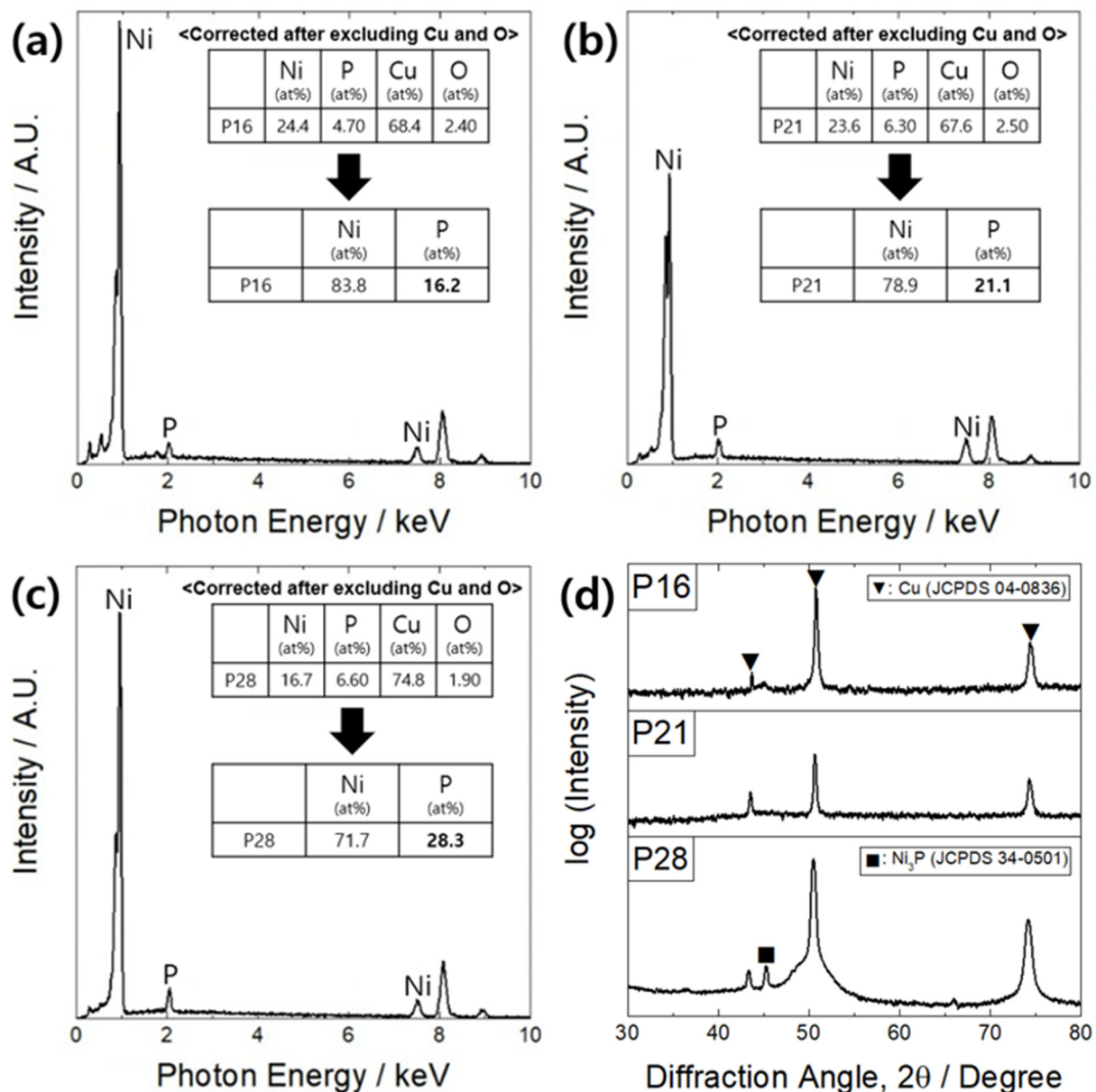


Figure 2. EDS spectra together with chemical composition ratios of the nickel phosphide thin films: (a) sample P16, (b) sample P21, and (c) sample P28. (d) represents their XRD patterns.

The crystal structure analysis for the Ni-P thin films is shown in Figure 2d. In the specimens of P16 and P21, only the signal for the copper substrate was detected, indicating that they had an amorphous crystal structure, whereas the P28 thin film had an additional tiny signal for the Ni₃P phase, strongly implying that the deposit was partially crystallized to form in the film crystallite phase adjacent to amorphous regions. According to the literature, when synthesizing Ni-P using electroplating, phosphorus atoms are included in the nickel lattice, preventing the growth of Ni-P crystals. As a result, the Ni-P plating layer gradually becomes a fine-grained or amorphous crystal structure. In particular, when the phosphorus content in the plating layer is 14–20 at% or more, the Ni-P plating layer becomes amorphous [23,41]. The thin films fabricated in this study contained more than 16 at% phosphorus, and all of them had, overall, an amorphous crystal structure, consistent with the report in the literature. Nevertheless, a more in-depth analysis is needed to explore any presence of crystalline phase in Ni-P electro-deposits with high phosphorus content (e.g., around 26 at% and higher).

3.2. Dependence of Electrochemical Properties on Phosphorus Content of Ni-P Thin Films

Figure 3a–c show the charge and discharge curves for the first three cycles at a rate of 0.2 C (4.74, 6.38, and 8.84 $\mu\text{A cm}^{-2}$), obtained from the P16, P21, and P28 thin films, respectively. Considering the phosphorus content in the thin film (Figure 2a–c), the theoretical specific capacities of P16, P21, and P28 were calculated to be 237, 319, and 442 mAh g^{-1} , respectively. However, the first charge capacities determined by the experiments were 404, 672, and 680 mAh g^{-1} , which were larger than the theoretical ones. These high initial charge capacities were probably due to the side reaction that formed a solid electrolyte interface [51]. After the first charge, a reversible charge–discharge response was observed. The initial discharge capacities of the three electrodes were 240, 300, and 342 mAh g^{-1} . Notably, the P28 specimen, which had the highest phosphorus content, showed approximately 77% of the theoretical capacity, which is comparable to that of commercial graphite. In addition, its volumetric capacity was estimated to be 2799 mAh cm^{-3} , which was about 3.3 times the theoretical value of graphite (850 mAh cm^{-3}). For all the electrodes, voltage plateau regions (or inflection points) were observed around 0.65 and 1.5 V vs. Li^+/Li on the charge curve, and around 1.3 and 2.0 V vs. Li^+/Li on the discharge curve (see inset figure (dQ/dV curve)). It is known that the former was the result of lithiation and delithiation, which involve Li_3P formation and decomposition reactions, and the latter was the result of the formation and decomposition reactions of an intermediate Ni_{12}P_5 compound [30].

Figure 4 shows the coulombic efficiency and discharge capacity retention rate with the number of charge/discharge cycles at a 0.2 C rate. After about three cycles in which irreversible surface products were formed, the P21 and P28 electrodes showed coulombic efficiencies of approximately 95% or more and operated stably. After 20 cycles, the capacity retention rates were approximately 81% (241 mAh g^{-1}) and 86% (293 mAh g^{-1}) of the initial capacities, respectively. However, the P16 electrode, which had the lowest phosphorus content, deteriorated rapidly from the beginning of cycling. These results are contrary to the general expectation that the cycling stability would deteriorate as a result of the volume change during charge/discharge with the increase in phosphorus content in the Ni-P electrode. The reason for this interesting result could be understood by comparing the surface changes of the three electrodes after the cycles.

Figure 5 shows the surface morphology of each electrode after 20 cycles. Electrodes P21 and P28 showed minor physical changes even after 20 cycles (Figure 5b,c), whereas the P16 electrode with low phosphorus content showed the partial detachment of active material, and several cracks were formed around the area where the detachment occurred (Figure 5a). This result implies that the relatively low cycling stability of the P16 electrode was caused by physical damage to the active materials. It was previously mentioned that a high reduction current density applied during the P16 electrode's fabrication could generate more hydrogen gas on the substrate surface, forming more voids between the substrate and thin film and reducing the adhesion between them (Figure 1). The adhesion test results confirmed that the P16 specimen, which had a low phosphorus content, had the worst adhesion (Figure 6). Thus, the electrode with a high P content had relatively severe stress changes in the thin film due to the volume change, but the high adhesion between the substrate and thin film prevented the thin film from being detached. On the other hand, the electrode with a low P content suffered detachment and severe electrode deterioration due to insufficient adhesion between the substrate and thin film despite the relatively small stress changes.

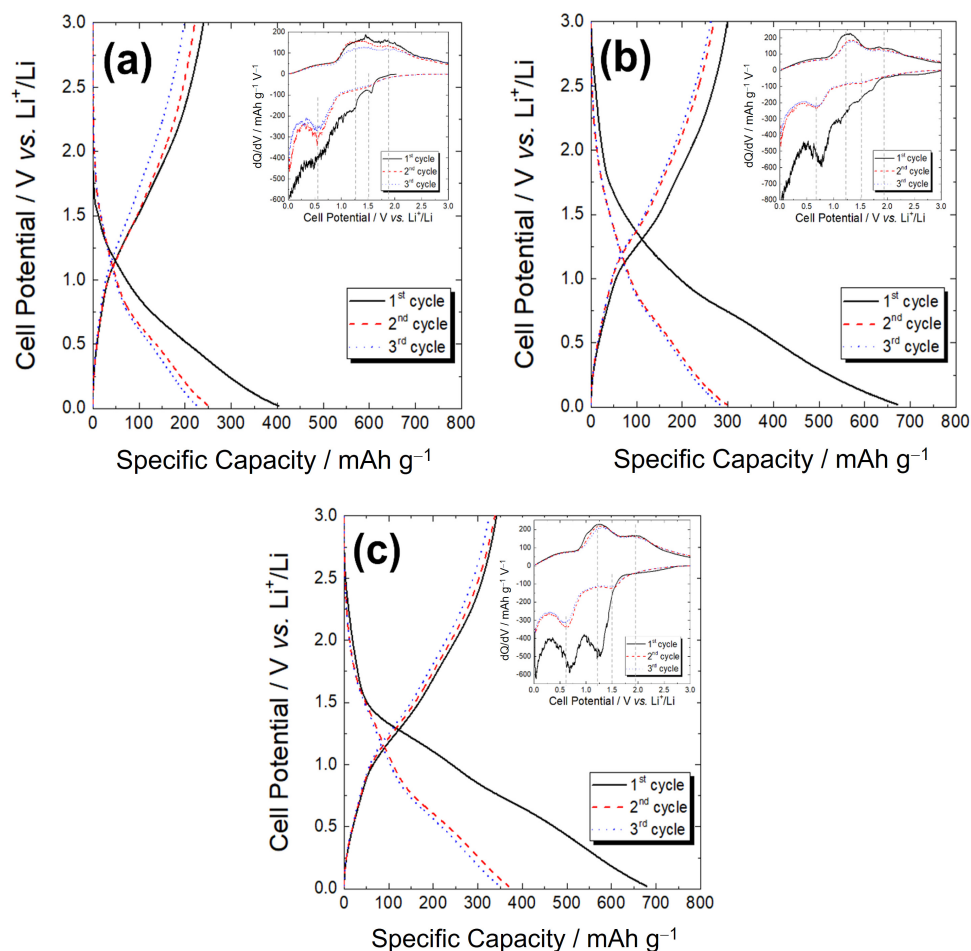


Figure 3. Charge and discharge curves for the first three cycles at a rate of 0.2 C (4.74, 6.38, and 8.84 $\mu\text{A cm}^{-2}$): (a) sample P16, (b) sample P21, and (c) sample P28 (28 at% P).

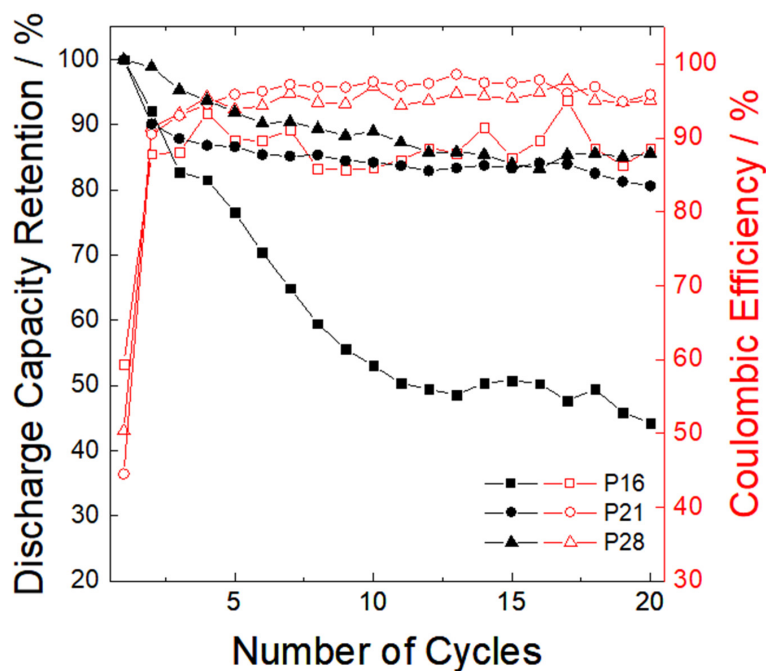


Figure 4. Variations in discharge capacity retention and coulombic efficiency with charge–discharge cycle at a rate of 0.2 C.

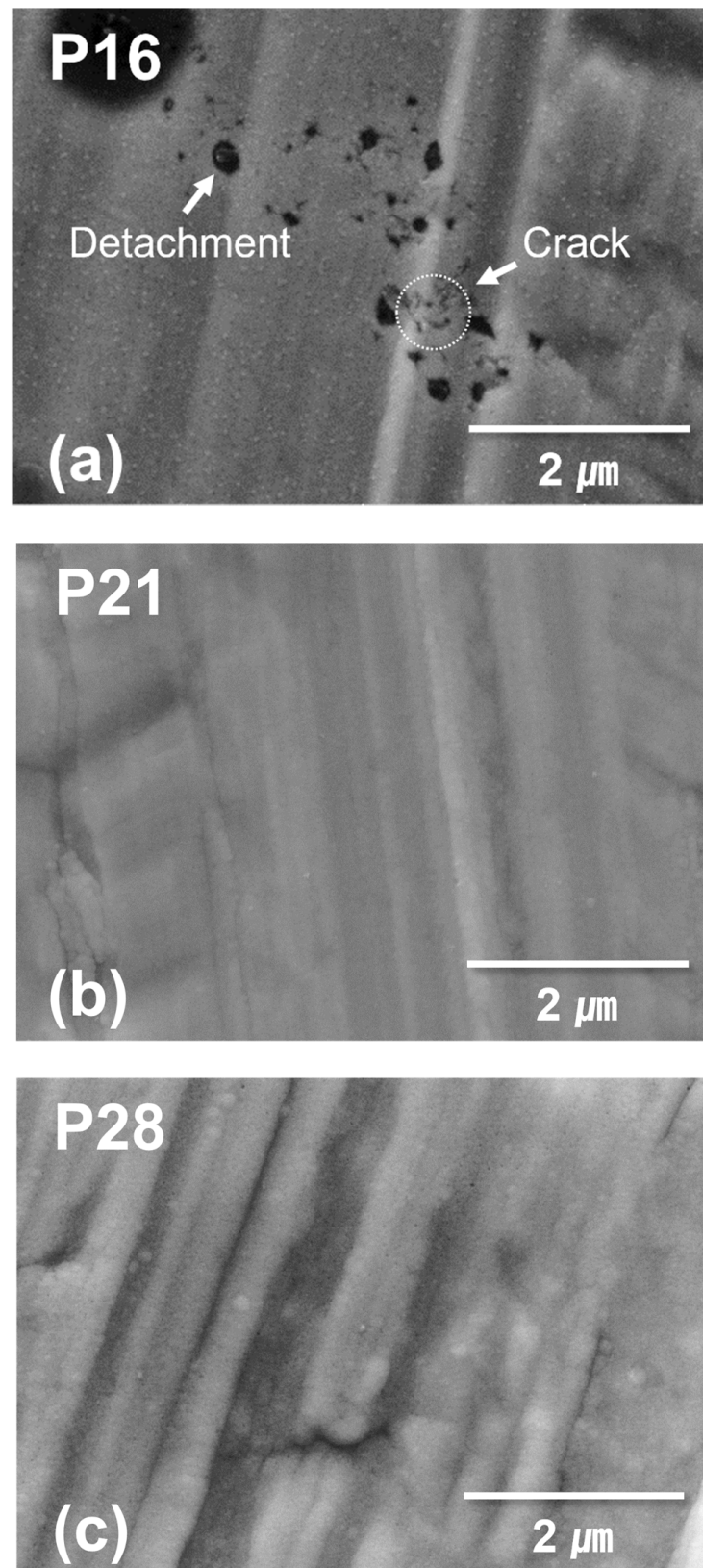


Figure 5. Scanning electron micrographs of the nickel phosphide thin films after 20 charge/discharge cycles: (a) sample P16, (b) sample P21, and (c) sample P28.

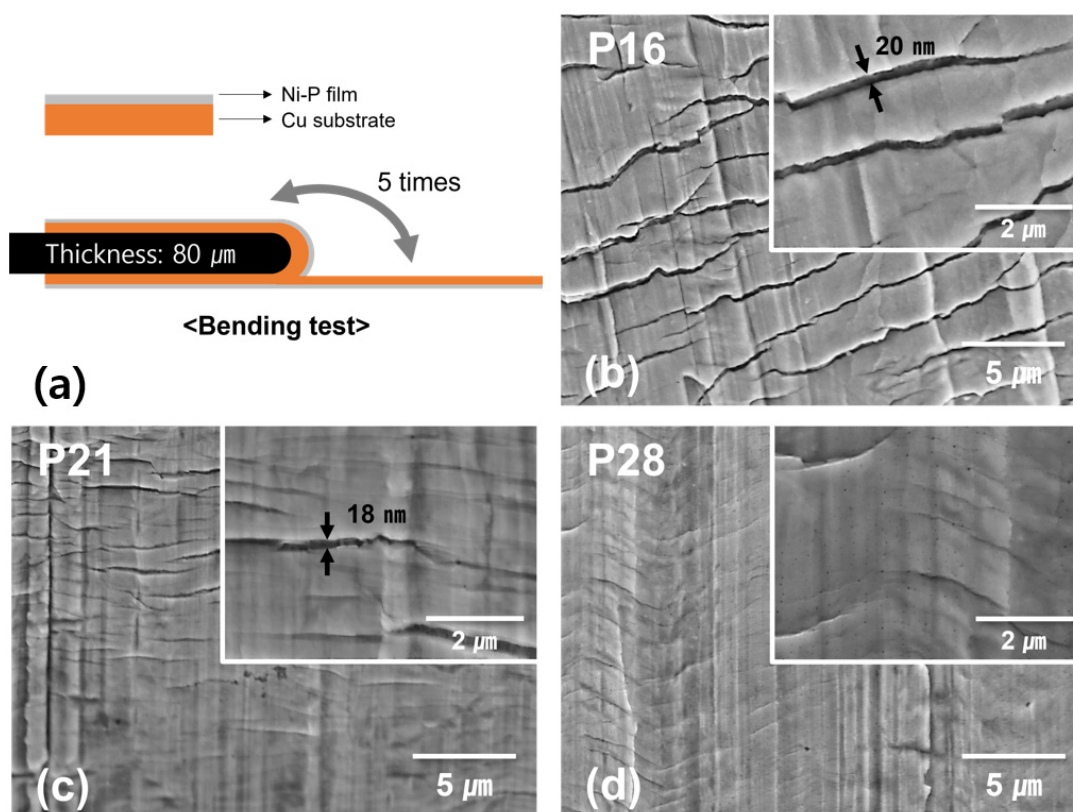


Figure 6. Bending test results for the qualitative analysis of the adhesion between the substrate and thin films: (a) schematic of bending test. Scanning electron micrographs of the nickel phosphide thin films after five repetitive bending cycles: (b) sample P16, (c) sample P21, and (d) sample P28.

3.3. Effect of Surface Morphology

The initial and cycling characteristics of the Ni-P electrodes explained in Section 3.2 show that relatively excellent characteristics could be obtained with a higher phosphorus content. However, the initial discharge capacity (342 mAh g^{-1}) remained at 77% of the theoretical one (442 mAh g^{-1}), indicating that the entire plated thin film was not effectively utilized for lithium storage. It is quite likely that such a low specific capacity might be caused by the low electrical conductivity and high reaction overvoltage of typical phosphide electrodes. Thus, this study tried to improve it by changing the surface structure. In particular, an attempt was made to increase the thin film utilization rate by modifying the surface to be more open-structured and have a large surface area.

To change the surface morphology of the thin film, spherical micro-electrodeposits of Ni-P were created by electroplating. In a general Ni-P electrodeposition process, the Ni-P electro-deposit attains a spherical shape, because phosphorus and nickel are co-plated omni-directionally [52]. However, at this time, the plating of pure nickel, which has a planar growth feature, proceeds simultaneously. As a result, the overall electrodeposited layer is gradually changed from a spherical shape to a flat shape. On the other hand, it is known that when the plating solution contains NaCl (or when NaCl is generated by the reaction of the pH adjuster NaOH and $\text{NiCl}_2 \cdot 6\text{H}_2\text{O}$ in the plating solution), nickel could grow anisotropically [53]. This means that the plating position of nickel is significantly limited by the presence of NaCl; thus, nickel hardly interferes with the spherical growth of the neighboring Ni-P. In this respect, instead of using ammonia hydroxide, which is generally used for pH control, NaOH was used to form spherical electrodeposits on the surface in this study (sample number 4 in Table 1).

Except for the use of NaOH as a pH adjuster, other deposition conditions were basically determined by the trial and error method. In particular, as expected, it was experimentally confirmed that the density of spherical deposits increased with the concentration of P

source, reduction current density, and deposition time. However, the film morphology was changed to be flat when they exceeded certain values, most likely due to the over-growth of the flat plating layer. From numerous experiments, the concentrations of pH adjuster and P source, current density, and deposition time given in Table 1 were finally selected for the well-defined spherical electrodeposits. As for the acidity, it was also experimentally proved that the lower the acidity was, the more spherical was the deposit we obtained in the pH range of 1.2–1.8. However, since lower acidity led to more vigorous H₂ gas evolution and then less uniform deposits, pH was set to 1.5 for the uniform thin film formation.

Figure 7a,b show the surface and inclined views of a Ni-P thin film with the same phosphorus content (28 at%) as the P28 thin film partially covered with spherical electrodeposits (from now on referred to as P28_S). Unlike the P28 thin film with flat-surface morphology, P28_S had spherical electrodeposits with a diameter of approximately 150 nm formed on a thin and flat plating layer with a thickness of 50 nm. An image analysis showed that the density of the spherical electrodeposits was ca. $2.3 \times 10^9 \text{ cm}^{-2}$. Using these values of diameter and density, and further assuming that the spherical electrodeposits existed in a hemispherical shape on the surface (inset in Figure 7a), the surface area was roughly calculated to be approximately 1.7 times the area of the flat electrode. A compositional analysis showed that the thin film (P28_S) with the spherical electrodeposits had almost the same composition ratio as the flat thin film (P28) (Figure 7c), and the overall crystal structure was also amorphous except for the presence of Ni₃P phase (Figure 7d).

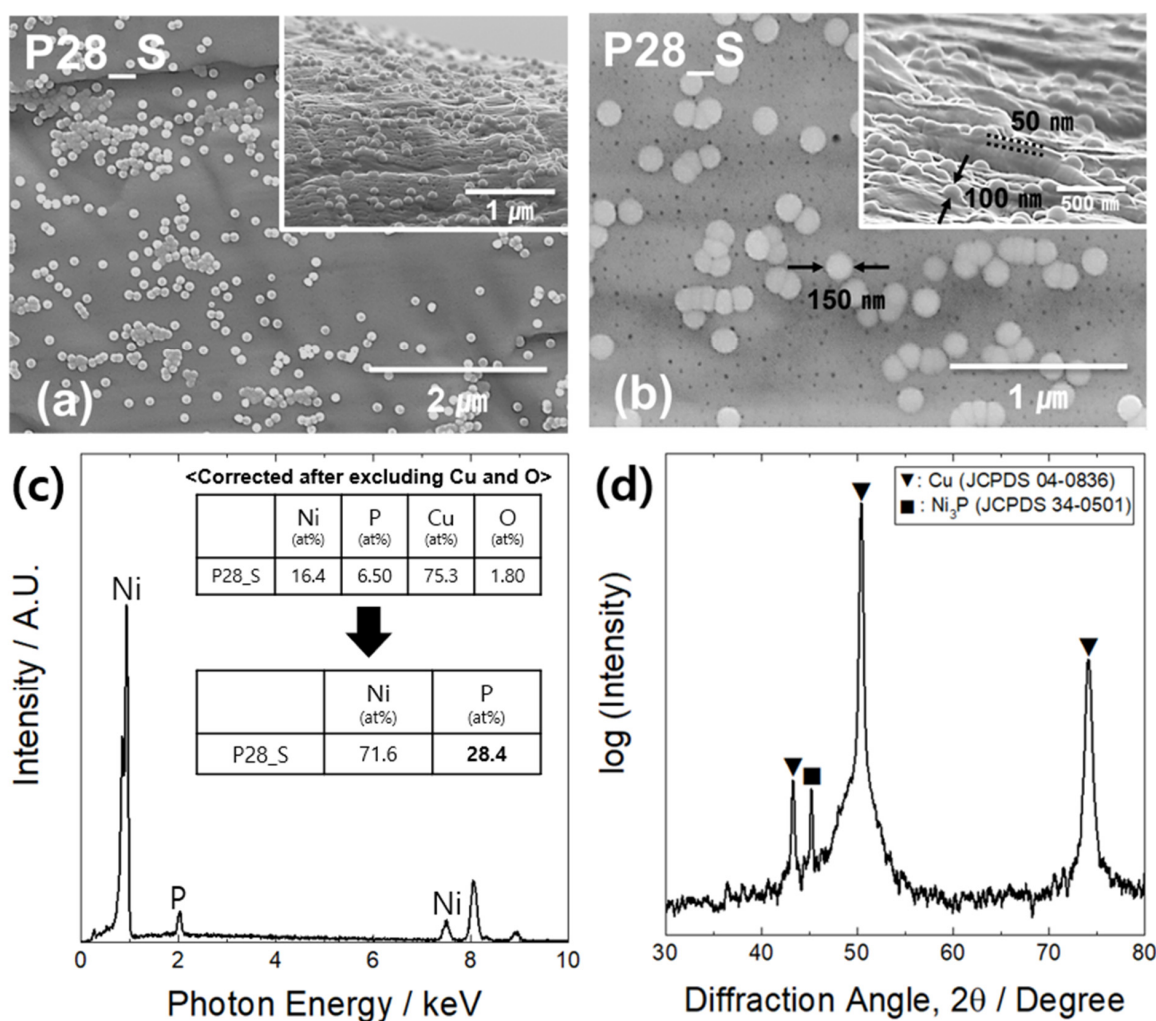


Figure 7. (a) Surface and inclined images of a Ni-P thin film partially covered with spherical electrodeposits (sample P28_S) and (b) their magnified images. (c,d) represent the EDS and XRD analyses of P28_S, respectively.

Figure 8 shows the results of evaluating the P28_S electrode as a negative electrode for a secondary lithium battery. Notably, the initial reversible discharge capacity reached as high as 445 mAh g^{-1} (Figure 8a). It is not yet apparent why the value slightly exceeded the theoretical capacity. It is likely that some of the oxides or surface products other than Ni-P also contributed to the capacity. It is not probable that there were any effects of the Cu substrate on the charge and discharge curves of the spherical-based Ni-P electrode, primarily due to the lack of exposure of the substrate. The cycling stability of the P28_S electrode (Figure 8b) was almost the same as that of the P28 electrode, except for a rather sharp decrease in the capacity during the initial charging and discharging. Compared with the P28 electrode, it had a 50 mAh g^{-1} larger capacity over the entire cycle. After charging and discharging 20 times, the specific discharge capacity of P28_S was 341 mAh g^{-1} , which was 1.2 times larger than that of the P28 electrode. Figure 8c shows the results of the rate performance test. As the discharge rate increased, the difference in the capacity retention rate became larger. At a 0.5 C rate, the P28 and P28_S electrodes showed capacity retention values of 69% and 74%, respectively, with values of 47% and 57% at a 1 C rate. An open structure and a large surface area of the P28_S electrode and the resulting high surface reaction rate might have been responsible for the improved high-rate characteristics compared with the P28 electrode. The rate performance of the P28_S electrode was equal to or greater than that of the Ni-P electrode reported previously [28].

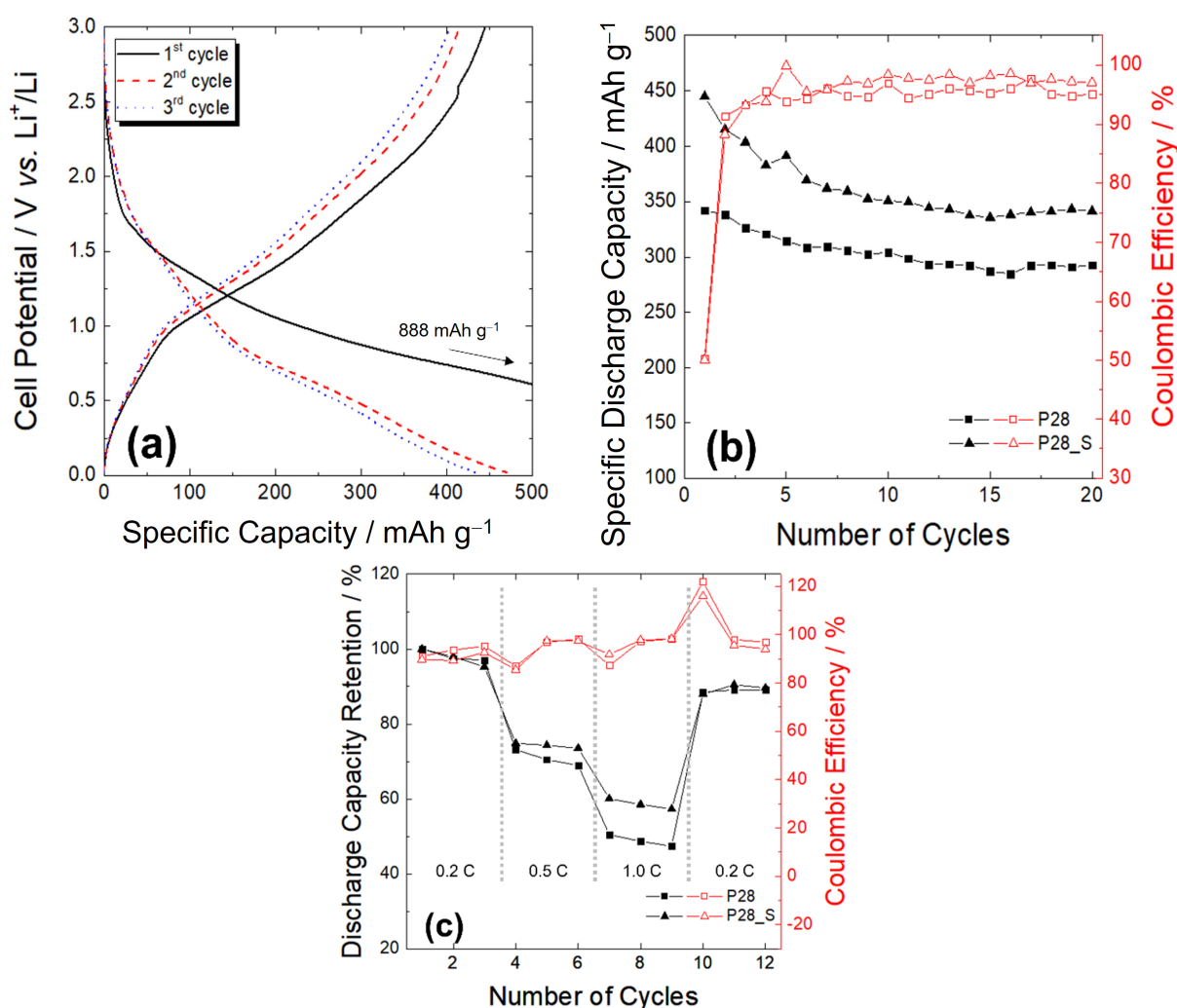


Figure 8. (a) Charge and discharge curves for the first three cycles at a rate of 0.2 C, obtained from the sample P28_S. (b) Variations in discharge capacity retention and coulombic efficiency with charge-discharge cycle at a rate of 0.2 C for samples P28 and P28_S. (c) Comparison of their rate capability.

4. Conclusions

In this work, amorphous nickel phosphide (Ni-P) thin films with various compositions were fabricated using electroplating and tested as anode materials for secondary lithium batteries. From the experimental results, the following conclusions were drawn:

1. Uniform, flat amorphous Ni-P thin films containing 16–28 at% phosphorus were successfully synthesized under different plating conditions. Interfacial cracks between the substrate and the thin film were not observed in high phosphorus content layers but lower phosphorus content resulted in severe interfacial cracks. This is most likely because more hydrogen gas was generated on the surface of the substrate; thus, more voids were formed between the substrate and thin film under the high reduction current applied when a thin film with a low phosphorus content was created;
2. As anodes for secondary lithium batteries, a higher phosphorus content for the thin film resulted in a higher specific capacity in general. In particular, when the phosphorus content was the highest (28 at%), the initial discharge capacity was 342 mAh g⁻¹, which was approximately 77% of the expected theoretical value. This is comparable to the theoretical specific capacity of commercially available graphite. Moreover, the capacity per volume was more than three times that of graphite;
3. The cycling stability of the thin film was improved as the phosphorus content increased. This was contrary to the general expectation that an increase in the phosphorus content would cause the cycling stability to deteriorate. This occurred because the electrode with high phosphorus content had high adhesion between the substrate and thin film, which prevented thin film separation, even with a significant stress change, whereas, because the electrode with low phosphorus content had poor adhesion between the substrate and thin film, severe separation and electrode deterioration occurred even with a relatively minor stress change;
4. To improve the specific capacity by increasing the utilization rate of the thin film, a Ni-P thin film containing fine spherical electrodeposits on the surface and high phosphorus content (28 at%) was fabricated. The initial specific discharge capacity was comparable to the theoretical specific capacity (445 mAh g⁻¹). Even after 20 charge and discharge cycles, it showed a high specific capacity (341 mAh g⁻¹), which was 1.2 times that of a flat electrode with the same composition. In addition, at the relatively high discharge rates of 0.5 and 1.0 C, the discharge capacity retention rate was 5–10% higher than that of a flat electrode. Further work on the spherical electrodeposits with various densities, sizes, etc., would give a deeper understanding of their effect on the electrode characteristics for lithium battery anodes.

Author Contributions: Conceptualization, J.-Y.H. and H.-C.S.; Data curation, J.-Y.H.; Funding acquisition, H.-C.S.; Investigation, J.-Y.H.; Supervision, H.-C.S.; Writing—original draft, J.-Y.H.; Writing—review & editing, H.-C.S. All authors have read and agreed to the published version of the manuscript.

Funding: This work was supported by National Research Foundation (NFR-2018R1A5A1025594) of Ministry of Science and ICT, and was supported by the Materials Technology Institute at Pusan National University.

Institutional Review Board Statement: Not applicable.

Informed Consent Statement: Not applicable.

Data Availability Statement: The data that support the findings of this study are available on request from the corresponding author.

Conflicts of Interest: The authors declare no conflict of interest.

References

1. Hu, Y.-S.; Demir-Cakan, R.; Titirici, M.-M.; Müller, J.-O.; Schlögl, R.; Antonietti, M.; Maier, J. Superior Storage Performance of a Si@SiO_x/C Nanocomposite as Anode Material for Lithium-Ion Batteries. *Angew. Chem. Int. Ed.* **2008**, *47*, 1645–1649. [[CrossRef](#)] [[PubMed](#)]
2. Cabana, J.; Monconduit, L.; Larcher, D.; Palacín, M.R. Beyond Intercalation-Based Li-Ion Batteries: The State of the Art and Challenges of Electrode Materials Reacting Through Conversion Reactions. *Adv. Mater.* **2010**, *22*, E170–E192. [[CrossRef](#)] [[PubMed](#)]
3. Fergus, J.W. Recent developments in cathode materials for lithium ion batteries. *J. Power Sources* **2010**, *195*, 939–954. [[CrossRef](#)]
4. Yuan, L.-X.; Wang, Z.-H.; Zhang, W.-X.; Hu, X.-L.; Chen, J.-T.; Huang, Y.-H.; Goodenough, J.B. Development and challenges of LiFePO₄ cathode material for lithium-ion batteries. *Energy Environ. Sci.* **2010**, *4*, 269–284. [[CrossRef](#)]
5. Ji, L.; Lin, Z.; Alcoutlabi, M.; Zhang, X. Recent developments in nanostructured anode materials for rechargeable lithium-ion batteries. *Energy Environ. Sci.* **2011**, *4*, 2682–2699. [[CrossRef](#)]
6. Phadatare, M.; Patil, R.; Blomquist, N.; Forsberg, S.; Örtengren, J.; Hummelgård, M.; Meshram, J.; Hernández, G.; Brandell, D.; Leifer, K.; et al. Silicon-Nanographite Aerogel-Based Anodes for High Performance Lithium Ion Batteries. *Sci. Rep.* **2019**, *9*, 14621. [[CrossRef](#)]
7. Huggins, R.A. Lithium alloy negative electrodes. *J. Power Sources* **1999**, *81*, 13–19. [[CrossRef](#)]
8. Zhao, J.; Zhang, Y.; Wang, Y.; Li, H.; Peng, Y. The application of nanostructured transition metal sulfides as anodes for lithium ion batteries. *J. Energy Chem.* **2018**, *27*, 1536–1554. [[CrossRef](#)]
9. Liu, X.; Huang, J.Q.; Zhang, Q.; Mai, L. Nanostructured Metal Oxides and Sulfides for Lithium-Sulfur Batteries. *Adv. Mater.* **2017**, *29*, 1601759. [[CrossRef](#)]
10. Xiang, J.; Tu, J.; Wang, X.; Huang, X.; Yuan, Y.; Xia, X.; Zeng, Z. Electrochemical performances of nanostructured Ni₃P–Ni films electrodeposited on nickel foam substrate. *J. Power Sources* **2008**, *185*, 519–525. [[CrossRef](#)]
11. Zuo, X.; Zhu, J.; Müller-Buschbaum, P.; Cheng, Y.-J. Silicon based lithium-ion battery anodes: A chronicle perspective review. *Nano Energy* **2017**, *31*, 113–143. [[CrossRef](#)]
12. Boyanov, S.; Bernardi, J.; Gillot, F.; Dupont, L.; Womes, M.; Tarascon, J.-M.; Monconduit, L.; Doublet, M.-L. FeP: Another Attractive Anode for the Li-Ion Battery Enlisting a Reversible Two-Step Insertion/Conversion Process. *Chem. Mater.* **2006**, *18*, 3531–3538. [[CrossRef](#)]
13. Cui, Y.-H.; Xue, M.-Z.; Fu, Z.-W.; Wang, X.-L.; Liu, X.-J. Nanocrystalline CoP thin film as a new anode material for lithium ion battery. *J. Alloys Compd.* **2013**, *555*, 283–290. [[CrossRef](#)]
14. Xiang, J.; Wang, X.; Zhong, J.; Zhang, D.; Tu, J. Enhanced rate capability of multi-layered ordered porous nickel phosphide film as anode for lithium ion batteries. *J. Power Sources* **2011**, *196*, 379–385. [[CrossRef](#)]
15. Lu, Y.; Tu, J.-P.; Xiong, Q.-Q.; Xiang, J.-Y.; Mai, Y.-J.; Zhang, J.; Qiao, Y.-Q.; Wang, X.-L.; Gu, C.-D.; Mao, S.X. Controllable Synthesis of a Monophase Nickel Phosphide/Carbon (Ni₅P₄/C) Composite Electrode via Wet-Chemistry and a Solid-State Reaction for the Anode in Lithium Secondary Batteries. *Adv. Funct. Mater.* **2012**, *22*, 3927–3935. [[CrossRef](#)]
16. Li, W.; Gan, L.; Guo, K.; Ke, L.; Wei, Y.; Li, H.; Shen, G.; Zhai, T. Self-supported Zn₃P₂ nanowire arrays grafted on carbon fabrics as an advanced integrated anode for flexible lithium ion batteries. *Nanoscale* **2016**, *8*, 8666–8672. [[CrossRef](#)]
17. Hall, J.W.; Membreno, N.; Wu, J.; Celio, H.; Jones, R.A.; Stevenson, K.J. Low-Temperature Synthesis of Amorphous FeP₂ and Its Use as Anodes for Li Ion Batteries. *J. Am. Chem. Soc.* **2012**, *134*, 5532–5535. [[CrossRef](#)]
18. Yang, D.; Zhu, J.; Rui, X.; Tan, H.; Cai, R.; Hoster, H.E.; Yu, D.Y.W.; Hng, H.H.; Yan, Q. Synthesis of Cobalt Phosphides and Their Application as Anodes for Lithium Ion Batteries. *ACS Appl. Mater. Interfaces* **2013**, *5*, 1093–1099. [[CrossRef](#)]
19. Chandrasekar, M.; Mitra, S. Thin copper phosphide films as conversion anode for lithium-ion battery applications. *Electrochim. Acta* **2013**, *92*, 47–54. [[CrossRef](#)]
20. Tarascon, J.-M.; Grugeon, S.; Laruelle, S.; Larcher, D.; Poizot, P. The Key Role of Nanoparticles in Reactivity of 3D Metal Oxides Toward Lithium. In *Lithium Batteries*; Springer: Boston, MA, USA, 2009; pp. 220–246. [[CrossRef](#)]
21. Gillot, F.; Boyanov, S.; Dupont, L.; Doublet, M.-L.; Morcrette, M.; Monconduit, L.; Tarascon, J.-M. Electrochemical Reactivity and Design of NiP₂ Negative Electrodes for Secondary Li-Ion Batteries. *Chem. Mater.* **2005**, *17*, 6327–6337. [[CrossRef](#)]
22. Boyanov, S.; Annou, K.; Villevieille, C.; Pelosi, M.; Zitoun, D.; Monconduit, L. Nanostructured transition metal phosphide as negative electrode for lithium-ion batteries. *Ionics* **2007**, *14*, 183–190. [[CrossRef](#)]
23. Daly, B.P.; Barry, F.J. Electrochemical nickel–phosphorus alloy formation. *Int. Mater. Rev.* **2003**, *48*, 326–338. [[CrossRef](#)]
24. Bruce, P.G.; Scrosati, B.; Tarascon, J.-M. Nanomaterials for Rechargeable Lithium Batteries. *Angew. Chem. Int. Ed.* **2008**, *47*, 2930–2946. [[CrossRef](#)] [[PubMed](#)]
25. Lou, P.; Cui, Z.; Jia, Z.; Sun, J.; Tan, Y.; Guo, X. Monodispersed Carbon-Coated Cubic NiP₂ Nanoparticles Anchored on Carbon Nanotubes as Ultra-Long-Life Anodes for Reversible Lithium Storage. *ACS Nano* **2017**, *11*, 3705–3715. [[CrossRef](#)]
26. Malini, R.; Uma, U.; Sheela, T.; Ganesan, M.; Renganathan, N.G. Conversion reactions: A new pathway to realise energy in lithium-ion battery—review. *Ionics* **2008**, *15*, 301–307. [[CrossRef](#)]
27. Cruz, M.; Morales, J.; Sánchez, L.; Santos-Peña, J.; Martín, F. Electrochemical properties of electrodeposited nicked phosphide thin films in lithium cells. *J. Power Sources* **2007**, *171*, 870–878. [[CrossRef](#)]
28. Kim, C.; Kim, H.; Choi, Y.; Lee, H.A.; Jung, Y.S.; Park, J. Facile Method to Prepare for the Ni₂P Nanostructures with Controlled Crystallinity and Morphology as Anode Materials of Lithium-Ion Batteries. *ACS Omega* **2018**, *3*, 7655–7662. [[CrossRef](#)]

29. Lu, Y.; Gu, C.; Ge, X.; Zhang, H.; Huang, S.; Zhao, X.; Wang, X.; Tu, J.; Mao, S. Growth of nickel phosphide films as anodes for lithium-ion batteries: Based on a novel method for synthesis of nickel films using ionic liquids. *Electrochim. Acta* **2013**, *112*, 212–220. [[CrossRef](#)]
30. Xiang, J.; Wang, X.; Xia, X.; Zhong, J.; Tu, J. Fabrication of highly ordered porous nickel phosphide film and its electrochemical performances toward lithium storage. *J. Alloys Compd.* **2011**, *509*, 157–160. [[CrossRef](#)]
31. Lu, Y.; Tu, J.-P.; Gu, C.-D.; Wang, X.-L.; Mao, S.X. In situ growth and electrochemical characterization versus lithium of a core/shell-structured Ni₂P@C nanocomposite synthesized by a facile organic-phase strategy. *J. Mater. Chem.* **2011**, *21*, 17988–17997. [[CrossRef](#)]
32. Hassoun, J.; Panero, S.; Scrosati, B. Electrodeposited Ni–Sn intermetallic electrodes for advanced lithium ion batteries. *J. Power Sources* **2006**, *160*, 1336–1341. [[CrossRef](#)]
33. Saitou, M.; Okudaira, Y.; Oshikawa, W. Amorphous Structures and Kinetics of Phosphorous Incorporation in Electrodeposited Ni–P Thin Films. *J. Electrochem. Soc.* **2003**, *150*, C140–C143. [[CrossRef](#)]
34. Lin, C.S.; Lee, C.Y.; Chen, F.J.; Li, W.C. Structural Evolution and Internal Stress of Nickel-Phosphorus Electrodeposits. *J. Electrochem. Soc.* **2005**, *152*, C370–C375. [[CrossRef](#)]
35. Lelevic, A.; Walsh, F.C. Electrodeposition of Ni P alloy coatings: A review. *Surf. Coat. Technol.* **2019**, *369*, 198–220. [[CrossRef](#)]
36. Morales, J.; Sanchez, L.; Martín, F.; Ramos-Barrado, J.; Sánchez, M. Nanostructured CuO thin film electrodes prepared by spray pyrolysis: A simple method for enhancing the electrochemical performance of CuO in lithium cells. *Electrochim. Acta* **2004**, *49*, 4589–4597. [[CrossRef](#)]
37. Xiang, J.Y.; Tu, J.P.; Huang, X.H.; Yang, Y.Z. A comparison of anodically grown CuO nanotube film and Cu₂O film as anodes for lithium ion batteries. *J. Solid State Electrochem.* **2007**, *12*, 941–945. [[CrossRef](#)]
38. Lin, C.S.; Lee, C.Y.; Chen, F.J.; Chien, C.T.; Lin, P.L.; Chung, W.C. Electrodeposition of Nickel-Phosphorus Alloy from Sulfamate Baths with Improved Current Efficiency. *J. Electrochem. Soc.* **2006**, *153*, C387. [[CrossRef](#)]
39. Yuan, X.; Sun, D.; Yu, H.; Meng, H.; Fan, Z.; Wang, X. Preparation of amorphous-nanocrystalline composite structured Ni–P electrodeposits. *Surf. Coat. Technol.* **2007**, *202*, 294–300. [[CrossRef](#)]
40. Shi, L.; Sun, C.; Liu, W. Electrodeposited nickel–cobalt composite coating containing MoS₂. *Appl. Surf. Sci.* **2008**, *254*, 6880–6885. [[CrossRef](#)]
41. Bonino, J.-P.; Bruet-Hotellaz, S.; Bories, C.; Pouderoux, P.; Rousset, A. Thermal stability of electrodeposited Ni–P alloys. *J. Appl. Electrochem.* **1997**, *27*, 1193–1197. [[CrossRef](#)]
42. Guo, J.; Liu, Q.; Wang, C.; Zachariah, M.R. Interdispersed Amorphous MnO_x-Carbon Nanocomposites with Superior Electrochemical Performance as Lithium-Storage Material. *Adv. Funct. Mater.* **2011**, *22*, 803–811. [[CrossRef](#)]
43. Delmer, O.; Balaya, P.; Kienle, L.; Maier, J. Enhanced Potential of Amorphous Electrode Materials: Case Study of RuO₂. *Adv. Mater.* **2008**, *20*, 501–505. [[CrossRef](#)]
44. Zhang, H.; Lu, Y.; Gu, C.-D.; Wang, X.-L.; Tu, J.-P. Ionothermal synthesis and lithium storage performance of core/shell structured amorphous@crystalline Ni–P nanoparticles. *CrystEngComm* **2012**, *14*, 7942–7950. [[CrossRef](#)]
45. Liu, P.; Hao, Q.; Xia, X.; Lei, W.; Xia, H.; Chen, Z.; Wang, X. Hollow Amorphous MnSnO₃ Nanohybrid with Nitrogen-Doped Graphene for High-Performance Lithium Storage. *Electrochim. Acta* **2016**, *214*, 1–10. [[CrossRef](#)]
46. Liu, J.; Zheng, M.; Shi, X.; Zeng, H.; Xia, H. Amorphous FeOOH Quantum Dots Assembled Mesoporous Film Anchored on Graphene Nanosheets with Superior Electrochemical Performance for Supercapacitors. *Adv. Funct. Mater.* **2015**, *26*, 919–930. [[CrossRef](#)]
47. Ratzker, M.; Lashmore, D.; Pratt, K. Electrodeposition and Corrosion Performance of Nickel–Phosphorus Amorphous Alloys. *Plat. Surf. Finish* **1986**, *73*, 74–82.
48. Brenner, A.; Couch, D.; Williams, E. Electrodeposition of alloys of phosphorus with nickel or cobalt. *J. Res. Natl. Inst. Stand. Technol.* **1950**, *44*, 109. [[CrossRef](#)]
49. Okamoto, N.; Wang, F.; Watanabe, T. Adhesion of Electrodeposited Copper, Nickel and Silver Films on Copper, Nickel and Silver Substrates. *Mater. Trans.* **2004**, *45*, 3330–3333. [[CrossRef](#)]
50. Gabe, D.R. The role of hydrogen in metal electrodeposition processes. *J. Appl. Electrochem.* **1997**, *27*, 908–915. [[CrossRef](#)]
51. Goodenough, J.B.; Kim, Y. Challenges for Rechargeable Li Batteries. *Chem. Mater.* **2009**, *22*, 587–603. [[CrossRef](#)]
52. Yu, Q.; Zeng, Z.; Liang, Y.; Zhao, W.; Peng, S.; Han, Z.; Wang, G.; Wu, X.; Xue, Q. Ni–P synergetic deposition: Electrochemically deposited highly active Ni as a catalyst for chemical deposition. *RSC Adv.* **2015**, *5*, 27242–27248. [[CrossRef](#)]
53. Lee, J.M.; Jung, K.K.; Ko, J.S. Effect of NaCl in a nickel electrodeposition on the formation of nickel nanostructure. *J. Mater. Sci.* **2015**, *51*, 3036–3044. [[CrossRef](#)]